

Basilisk/Gerris Users' Meeting 2019



Bag-breakup – mechanism of sea spray
generation in strong winds

A.N. Zotova, Yu.I. Troitskaya,
D.A. Sergeev, A.A. Kandaurov

Institute of Applied Physics of the RAS, Department of geophysical research,
Nizhny Novgorod, Russian Federation

Sea spray

- typical phenomenon for the boundary layer of the atmosphere with a strong wind
- plays an important role in the transfer of heat and momentum
- It is difficult to estimate the number and size of droplets in a sea spray, because the mechanisms of its occurrence are poorly understood



Investigation of the spray generation mechanisms at high winds

The purposes:

- To investigate mechanisms responsible for spray generation at strong wind, classify them and quantify the efficiency of the disclosed mechanisms
- To construct the spray generation function at strong winds basing on disclosed mechanisms of their generation
- To estimate momentum and heat fluxes at storm winds taking into account the effect of spray

Experimental setup

The high-speed wind-wave flume of IAP, Nizhny Novgorod, Russia



- Dimensions of the channel 10m x 0.4m x 0.4 m
- the air-flow velocity corresponds to 10-m neutral wind speed U_{10} from 4 to 40 m/s

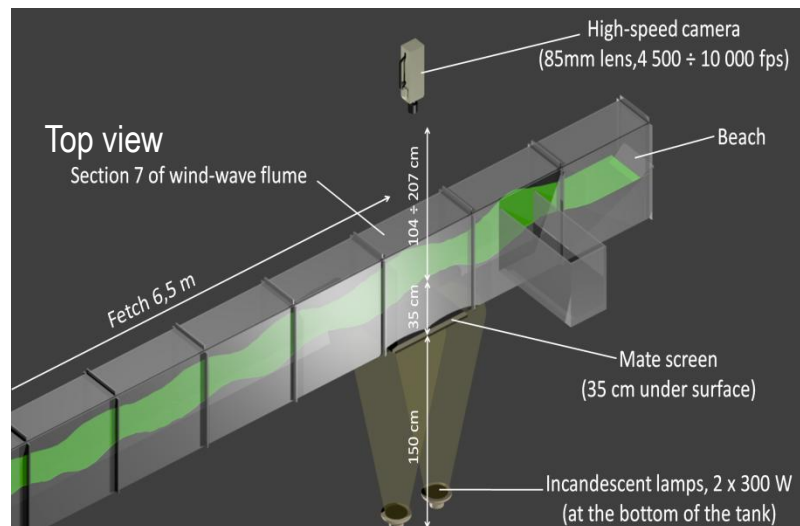
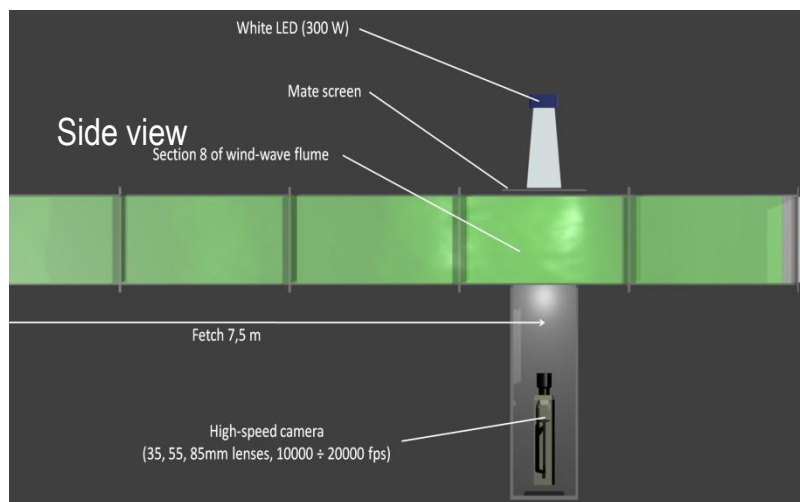
Annular wind-wave channel Aeolotron at the University of Heidelberg, Germany



- 60 cm width
- 2.4 m height
- circumference of 27.3 m at the inner wall
- water depth during experiments 1.0 m
- water volume 18.0 m³
- air space volume 24 m³

The main method: high speed photography through the transparent walls and upper lid of the channel

Experimental setup for the shadow method



MEMRECAM HX-3 High Speed Camera System



Memrecam HX3 High Resolution Mode

Max Res (pixels)	2560 X 1920	
Optical Format	35.20 mm	
fps @ Max Res	2,000	
	Mono	Color
ISO Rating	10,000	2,500

Memrecam HX3 High Speed Mode

Max Res (pixels)	1280 X 960	
Optical Format	35.20 mm	
fps @ Max Res	7,690	
	Mono	Color
ISO Rating	40,000	10,000

Memory Option	16GB, 32GB, 64GB	
Maximum fps	1,300,000	

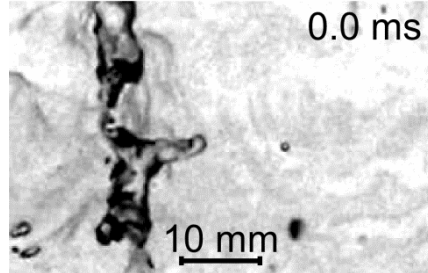
Complex structure of a wind – wave crest $U_{10}=29$ m/s

2500 fps, Nikkor35 f1.4, Distance = 100-140 cm



Investigation of details enabled us to specify 3 types of the spray generating phenomena

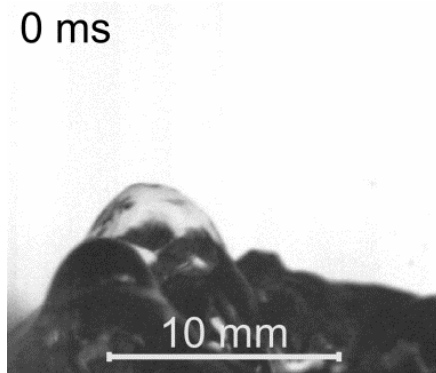
Spray generation mechanisms



Fragmentation of liquid ligaments (top view)

Wind speed
 $U_{10}=25.9$ m/s

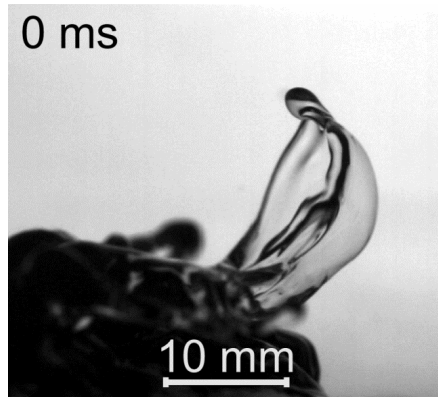
- $f = 85$ mm
- Samyang 85 mm f/1.4
- Distance = 65 cm
- Scale = $73 \mu\text{m}/\text{px}$
- 10000 fps



Bursting of the underwater bubble (side view)

Wind speed
 $U_{10}=27.8$ m/s

- $f = 55$ mm
- Samyang 85 mm f/1.4
- Distance = 65 cm
- Scale = $73 \mu\text{m}/\text{px}$
- 2000 fps



Bag breakup (side view)

Wind speed
 $U_{10}=27.8$ m/s

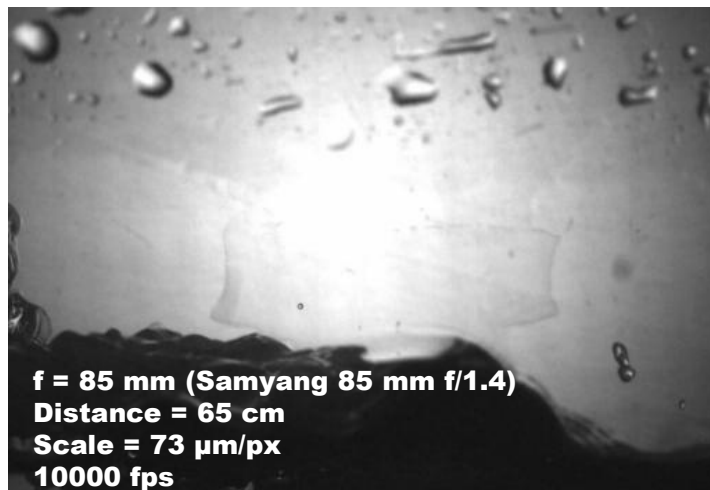
- $f = 55$ mm
- Samyang 85 mm f/1.4
- Distance = 65 cm
- Scale = $73 \mu\text{m}/\text{px}$
- 2000 fps

Spray generation at the wave crests (“bag breakup”)

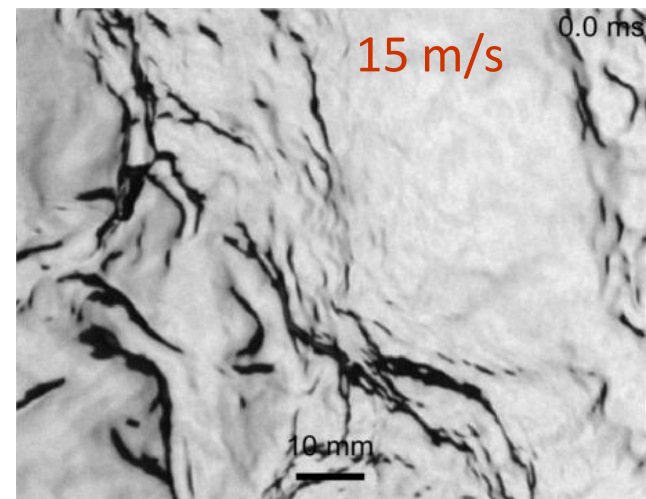
LASIF, Luminy, 250 fps, courtesy by H. Branger, 1990, 14 m/s



Wind speed $U_{10}=27.7$ m/s Width 74 mm



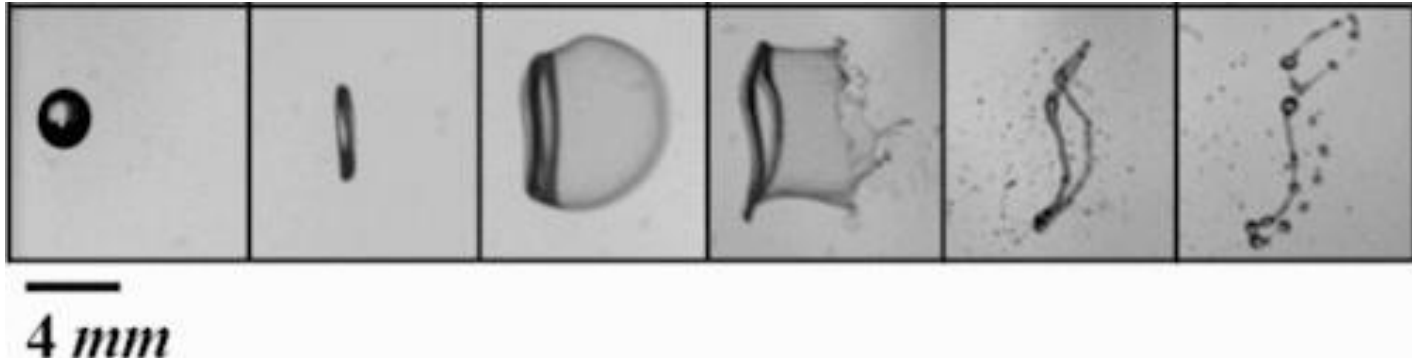
Aeolotron: The Heidelberg wind/wave facility



“Bag breakup”

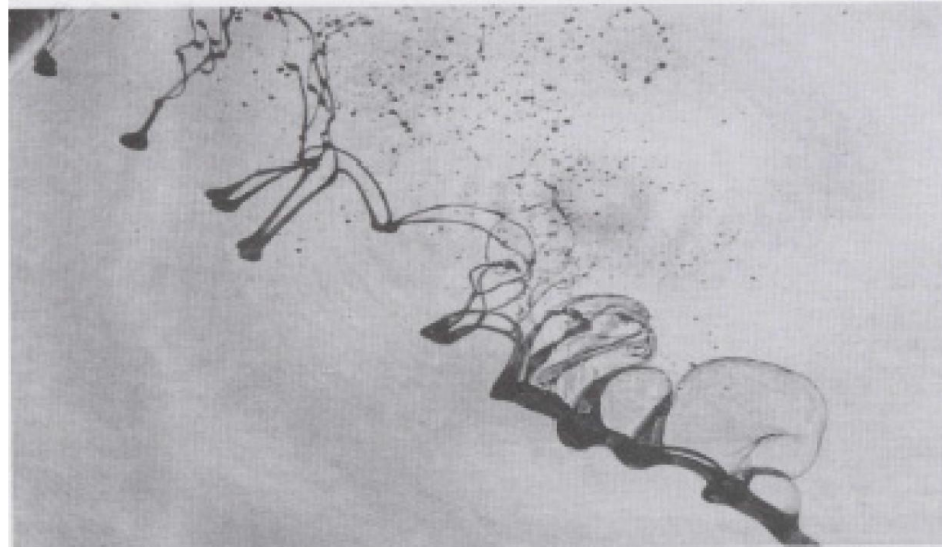
Bag-breakup mode of fragmentation of a droplet

V. Kulkarni and P. Sojka Phys. Fluids 26, 072103 (2014)

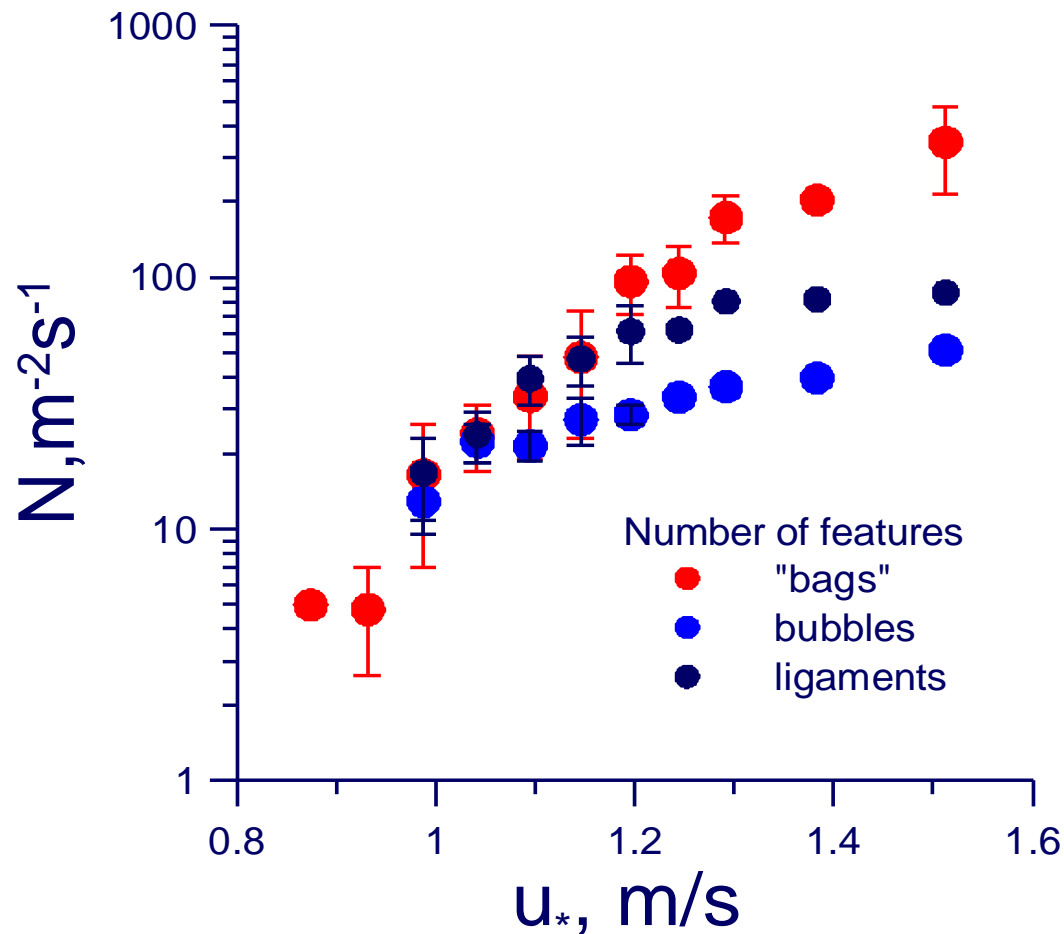


Bag-breakup of liquid jets in crossflow

Ashgriz, N. Atomization of a liquid jet in a crossflow. In Proceedings of the 4th International Meeting of Advances in Thermofluids, Melaka, Malaysia, 3–4 October 2011.



The specific number of spray generating events (per unit time per unit area) versus friction velocity



The number of the bag-breakup events dominates at high winds

“Bag-breakup” SGF

The size spectra of droplets produced by a sole bag

“Bags” generate spray in two ways

1. Rupturing the canopy of inflated bag



2. Fragmentation of the rim



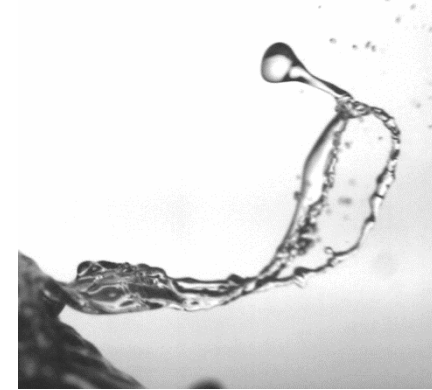
$$F_{drops}(r, R) = F_{film}(r, R) + F_{rim}(r, R)$$

Rupturing the canopy of inflated bag (similarly to bursting of an underwater bubble)



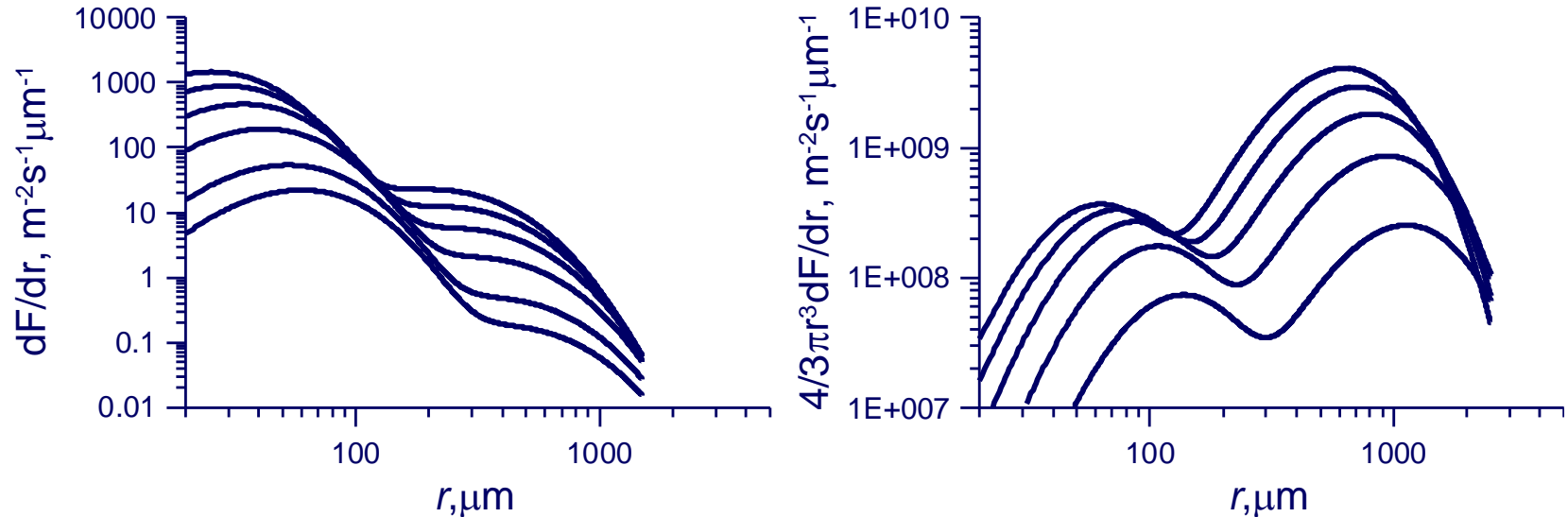
H. Lhuissier and E. Villermaux Bursting bubble aerosols J. Fluid Mech., V. 696, 2012, p. 5-44

Fragmentation of the bag rim (similarly to the fragmentation of the rim at of a droplet in gaseous flow)



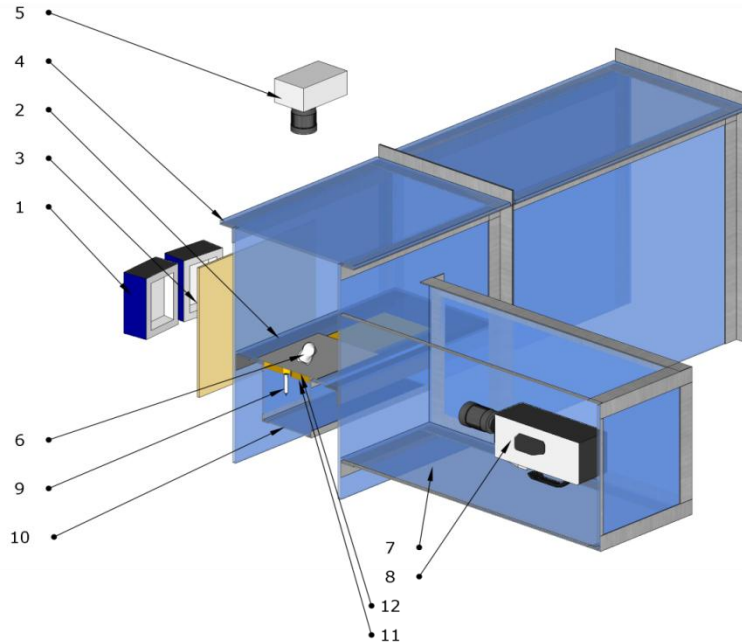
Chou WH, Faeth GM (1998) Temporal properties of secondary drop breakup in the bag breakup regime. Int J Multiphase Flow, 24:889–912

Bag breakup SGF in the lab for u^* from 1 m/s to 2 m/s with an increment 0.2 m/s



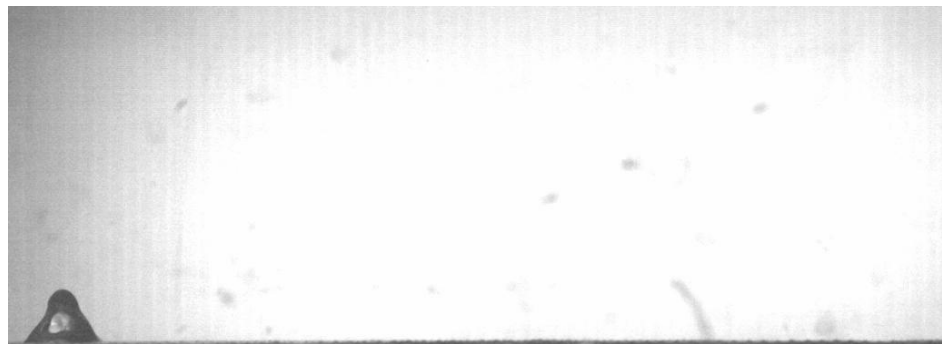
Y. Troitskaya et al., "The 'Bag Breakup' Spume Droplet Generation Mechanism at High Winds. Part I: Spray Generation Function," J. Phys. Oceanogr., vol. 48, no. 9, pp. 2167–2188, 2018.

The experimental setup for studying the mechanism of the spray production due to the bag-breakup fragmentation with the use of the artificial disturbance



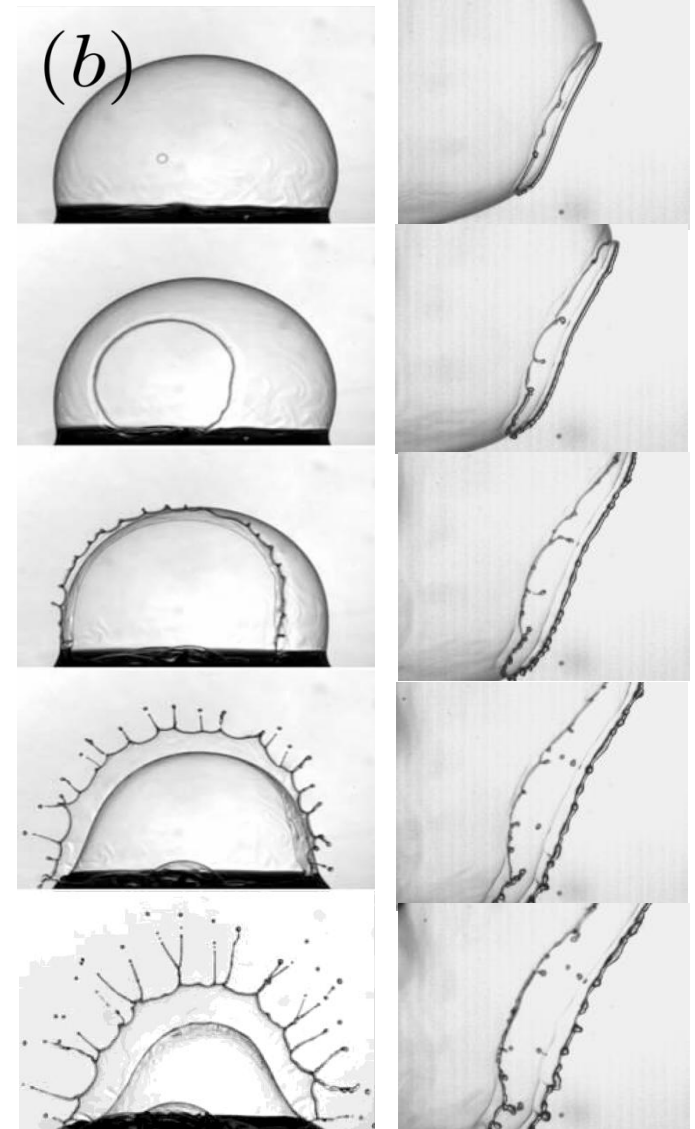
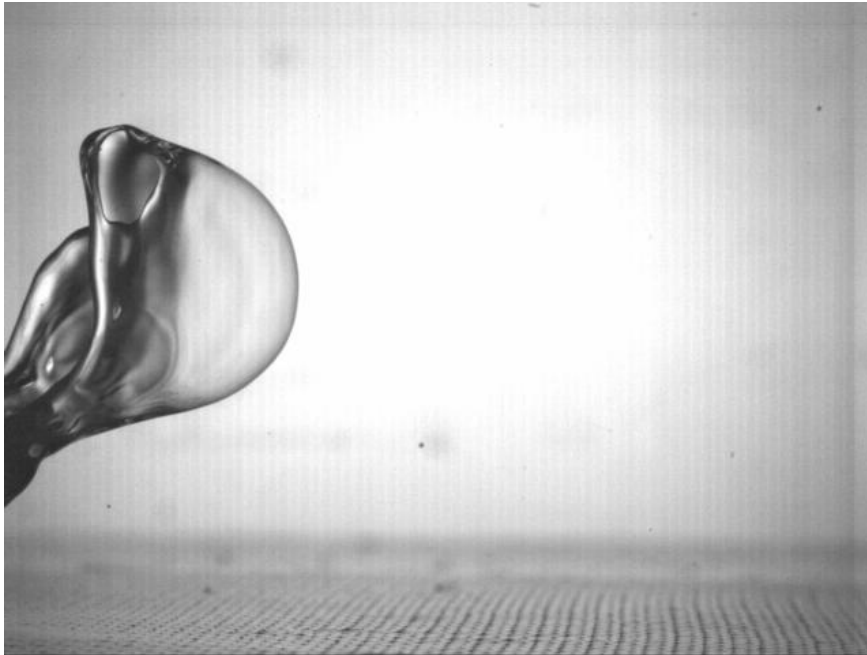
- 1 - LED lamps,
- 2 - solid flat bottom,
- 3 - matte screen,
- 4 - high-speed wind-wave channel,
- 5 - top-view camera,
- 6 - the "bag",
- 7 - nozzle,
- 8 - water tank,
- 9 - side channel box,
- 10 - side-view camera,
- 11 - foam rubber in water,
- 12 - nylon mesh.

Video from side-view camera for $u_* = 0.61$ m/s.



The canopy droplet production

Plateau-Rayleigh versus Rayleigh-Taylor instability



Left: Rayleigh-Taylor instability (H.Lhuissier, E.Villermaux
Bursting bubbles Phys. Fluids, 21, 09111-1 (2009))

$$\tau_{R-T} \sim \left(\frac{\sigma}{\rho_w \gamma^3} \right)^{1/4} \quad \gamma = V^2/R \quad V = \sqrt{\frac{2\sigma}{\rho_w h}}$$

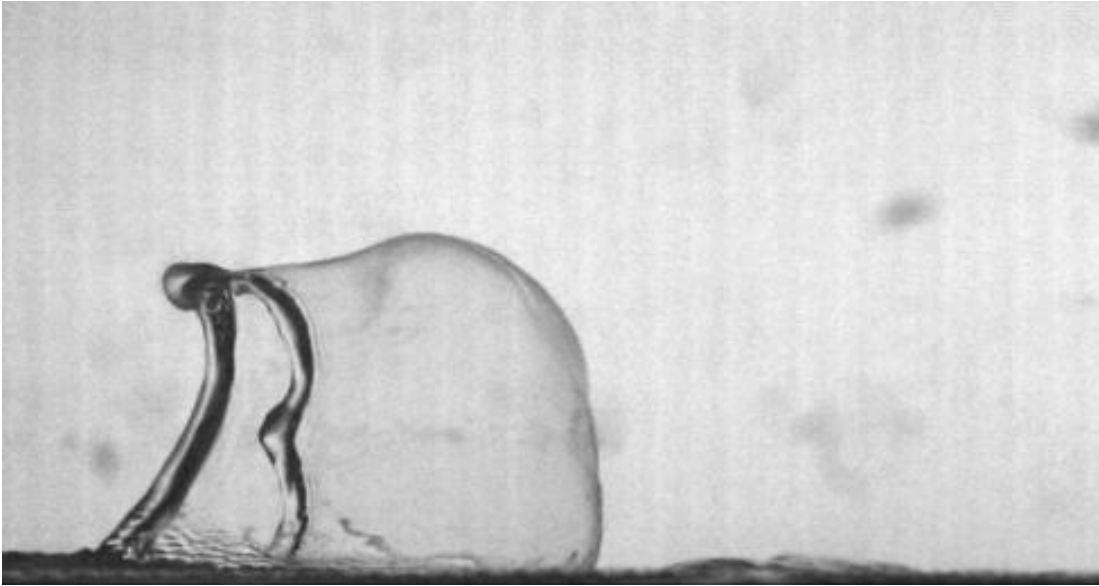
Right: Plateau-Rayleigh instability $\tau_{P-R} \sim \left(\frac{\rho_w \delta^3}{\sigma} \right)^{1/2} \quad \delta \sim h$

The P-R instability is faster than R-T one

$$\frac{\tau_{P-R}}{\tau_{R-T}} \sim \left(\frac{h}{R} \right)^{3/4} \ll 1$$

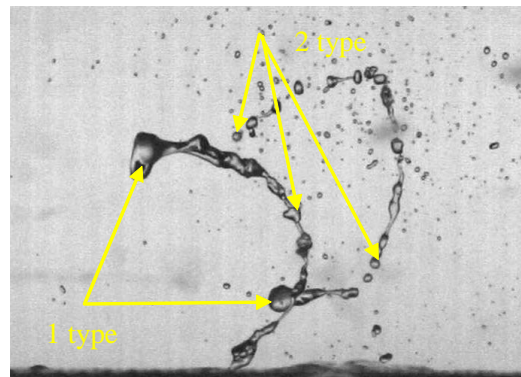
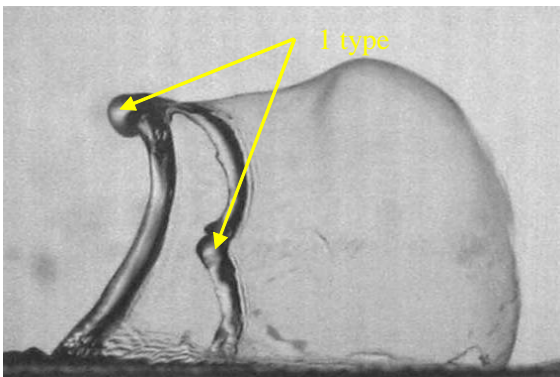
The rim droplet production

Droplet formation during fragmentation of the rim



Type 1 droplets

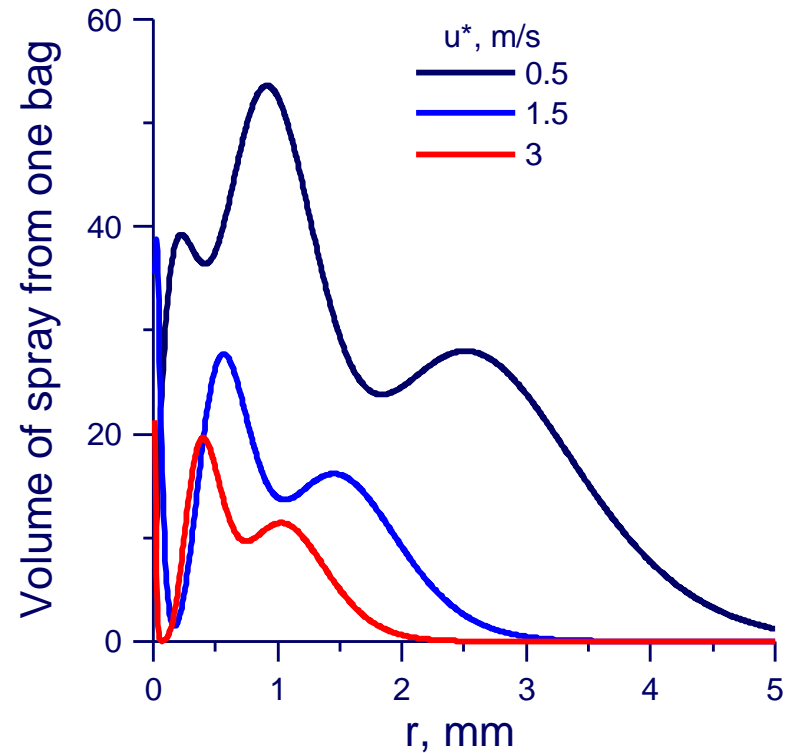
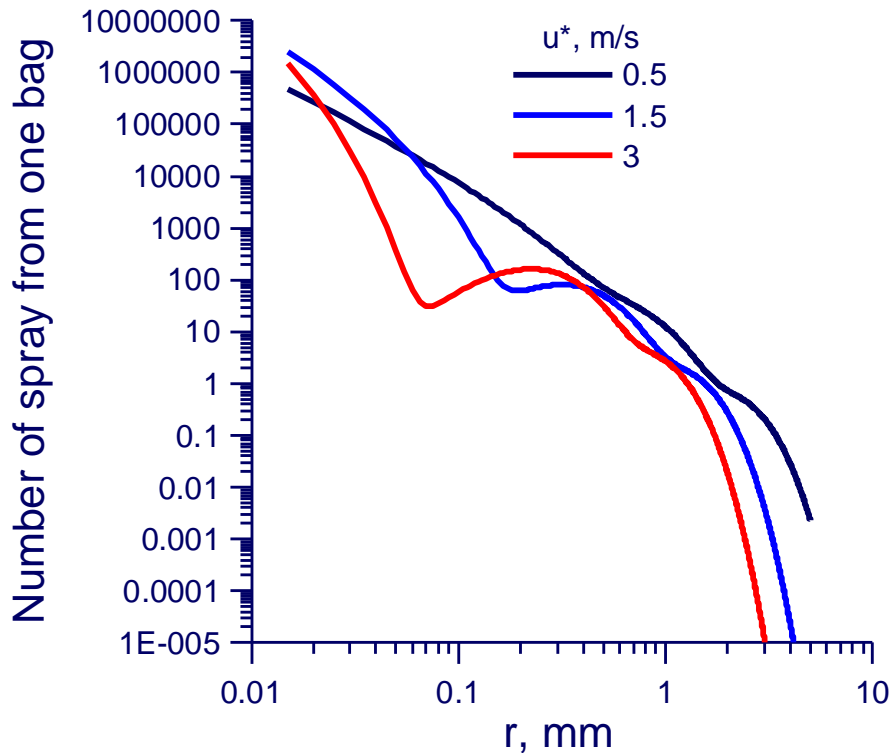
Small number of the large droplets formed as the result of development of the instability at the rear edge of the bag before the rupture of the canopy



Type 2 droplets

Smaller droplets formed due to the capillary (P-R) instability of the remaining rim

The size spectra of the droplets from one bag of a certain radius $R=20$ mm at different values of the wind friction velocity u_*

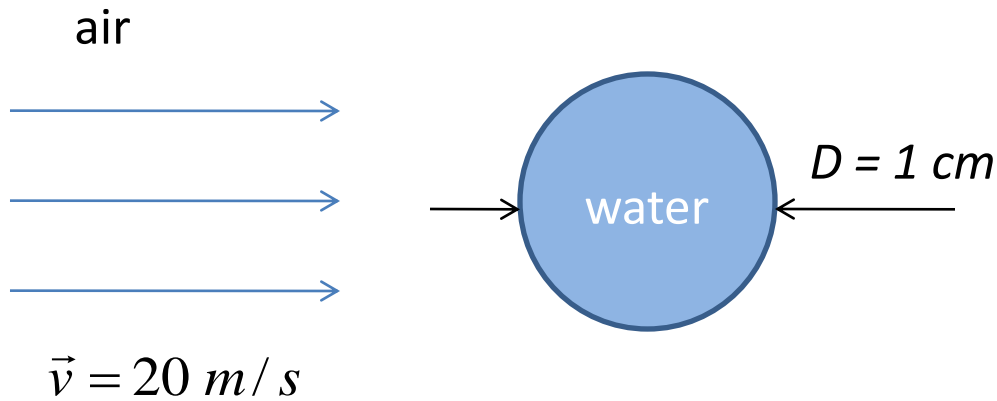


Open questions

- What is the mechanism for the formation of the perturbation from which bag evolves?
- What factors influence its size?
- How does the size of the disturbance and the wind speed affect the size of the canopy and the thickness of its film?
- What are the parameters of the bag and how do they affect the size of the droplets resulting from its rupture?

and so on ...

Configuration of the problem



$$We = \frac{\rho_a v^2 D}{\sigma}$$

$$Re = \frac{\rho_a D v}{\mu_a}$$

$$Oh_w = \frac{\mu_w}{(\rho_w D \sigma)^{1/2}}$$

$$\rho_w = 1000. \text{ kg/m}^3$$

$$\rho_a = 100. \text{ kg/m}^3$$

$$\mu_w = 1.003\text{e-}3 \text{ Pa}\cdot\text{s}$$

$$\mu_a = 1.8\text{e-}5 \text{ Pa}\cdot\text{s}$$

$$\sigma = 72.9\text{e-}3 \text{ N/m}$$

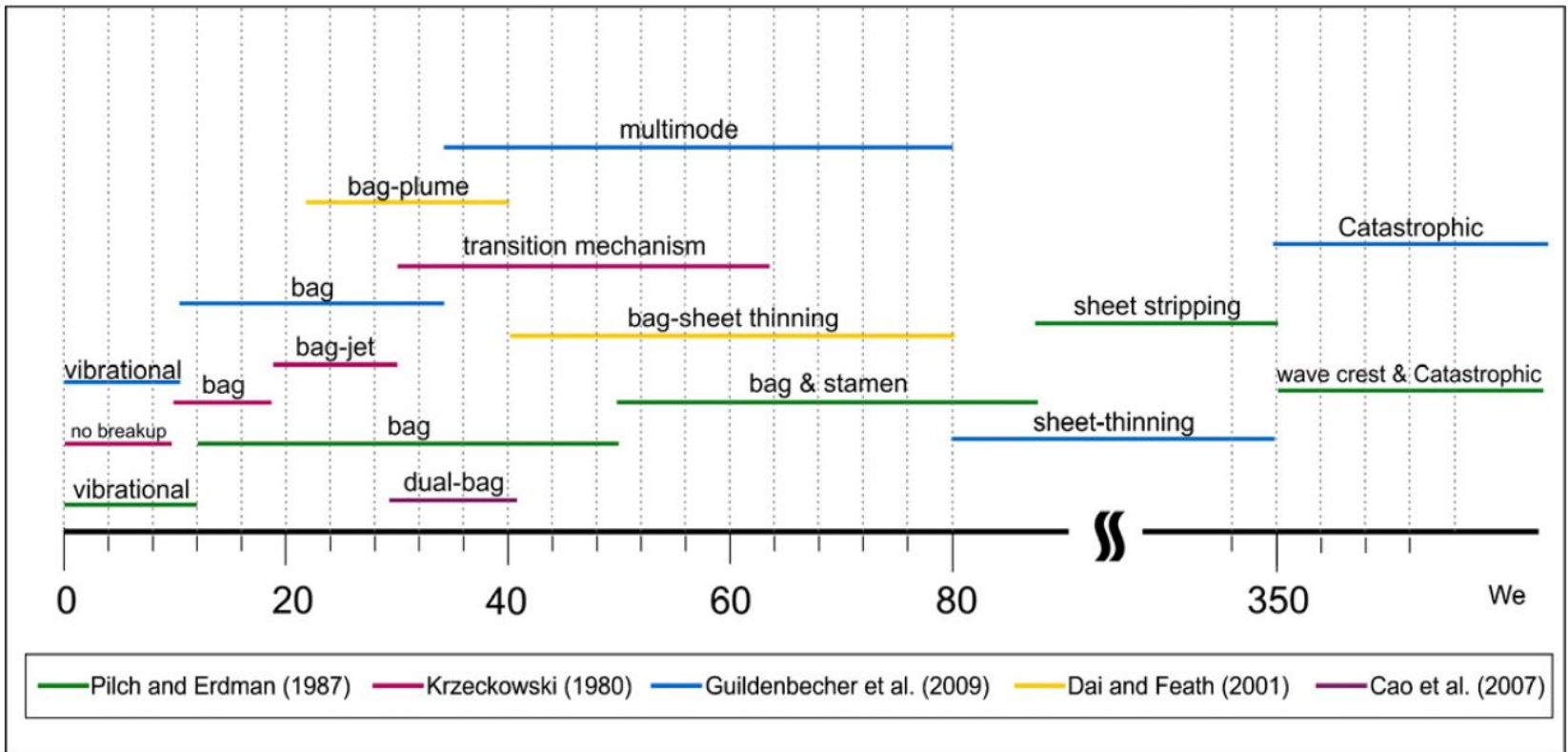


$$We = 55$$

$$Re = 11 \cdot 10^3$$

$$Oh_w = 10^{-3}$$

Breakup modes in terms of Weber number



M. Jalaal, K. Mehrvaran, 2012. Fragmentation of falling liquid droplets in bag breakup mode.
Int. J. Multiphase Flow 47: 115-132.

Parameters of the problem

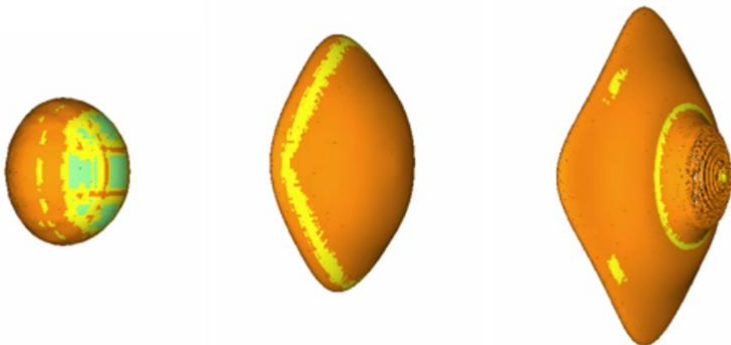
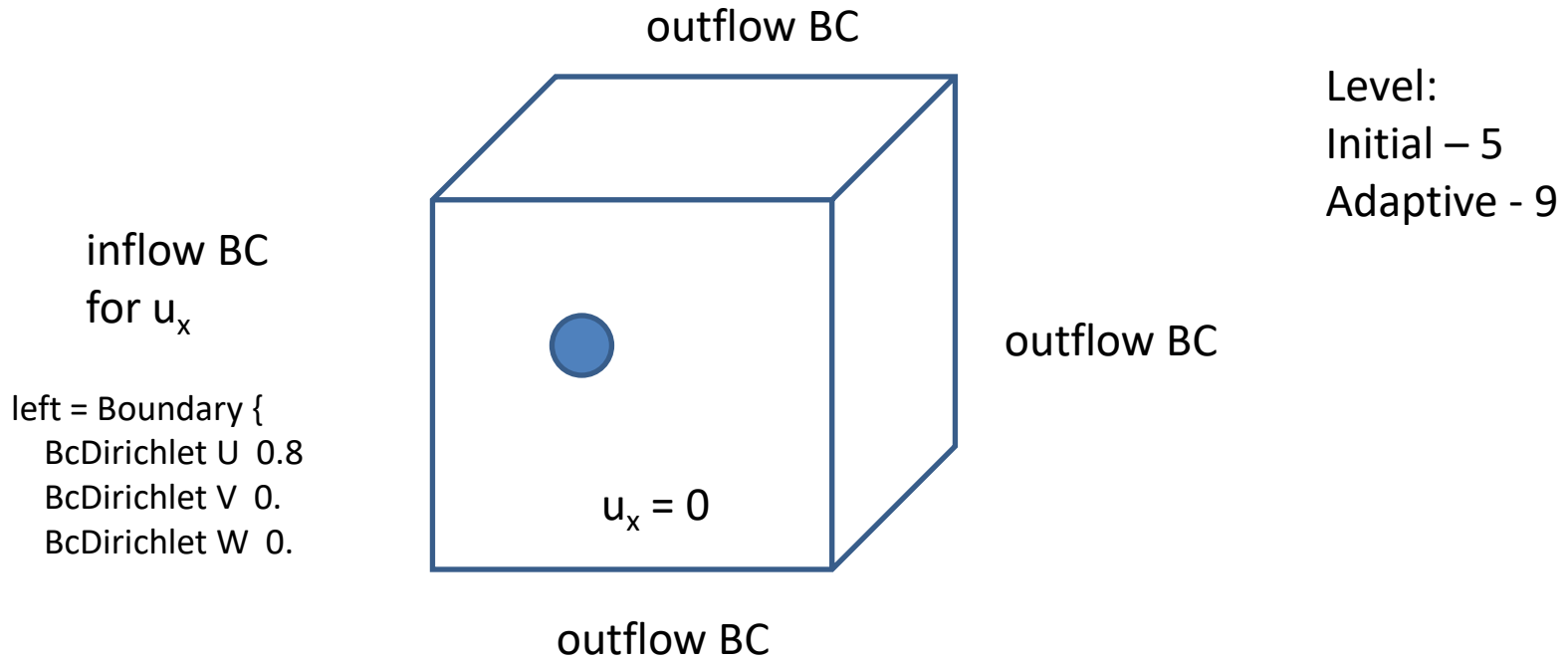
the lower ρ_a/ρ_w
the lower
computational
cost

$$\Rightarrow \rho^* = \frac{\rho_a}{\rho_w} = 1000 \Rightarrow \rho_a' = \rho_a \cdot 100 \Rightarrow \rho^{*'} = \frac{\rho_a'}{\rho_w'} = 10$$

The droplet destruction mechanism depends on the Weber number characterizing the system, so to keep the same Weber number we changed the value of the external medium velocity. In order to reduce the required resolution we changed the value of dynamic viscosity.

$$\text{Re} = \text{Re} \cdot 10 \leftarrow \left\{ \begin{array}{l} \rho_a' = \rho_a \cdot 100 \\ v' = v/10 \\ \mu_a' = \mu_a \cdot 100 \end{array} \right. \Rightarrow We = \text{const}$$

Results of direct numerical simulation in Gerris

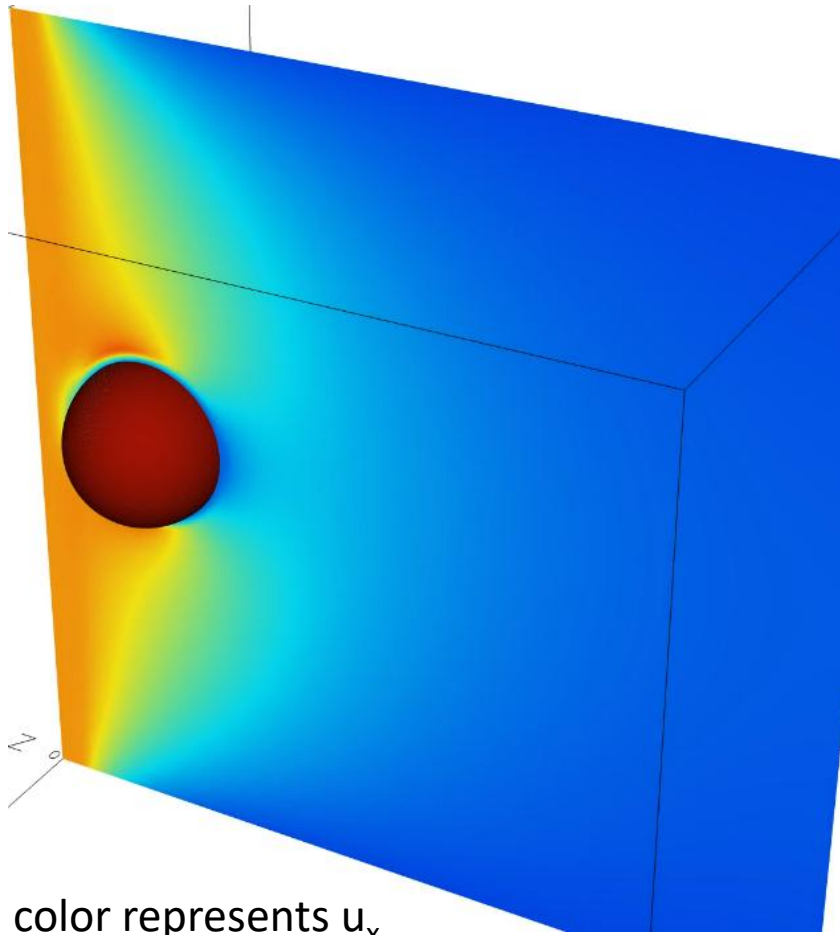


We corresponds to the initial problem numbers, Re reduced by a factor of 10 ($\rho_a' = \rho_a \cdot 100$; $v' = v/10$; $\mu_a' = \mu_a \cdot 100$; $\mu_w' = \mu_w \cdot 100$; $\sigma' = \sigma$).

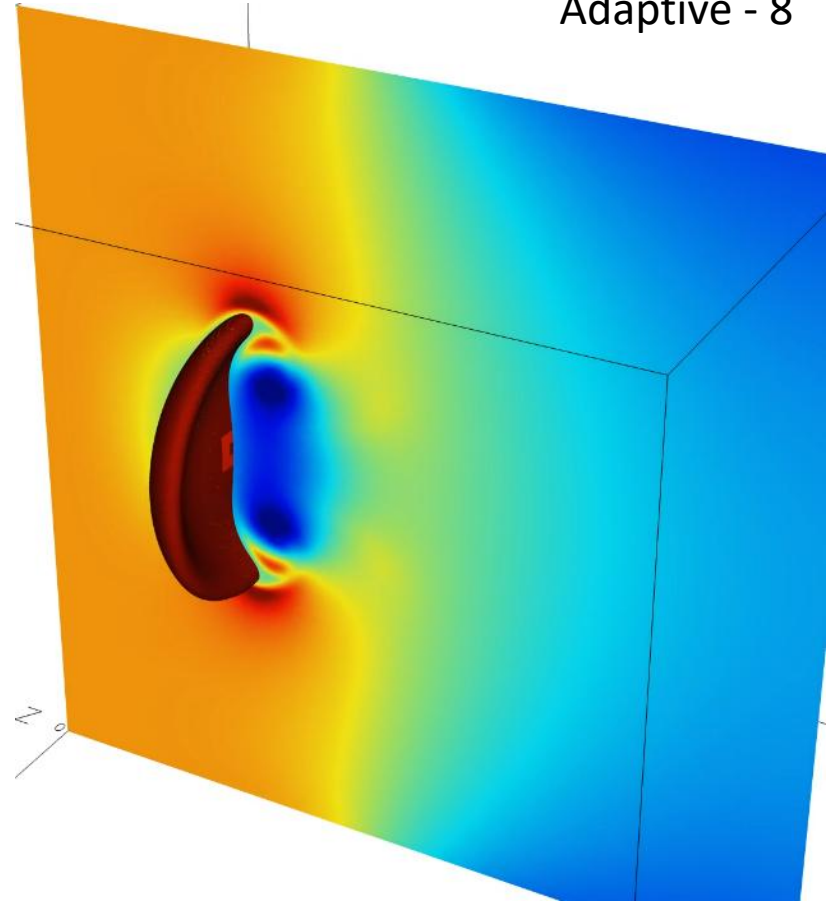
Results of direct numerical simulation in Basilisk

The same parameters and initial conditions as in Gerris, but...

Level:
Initial – 6
Adaptive - 8



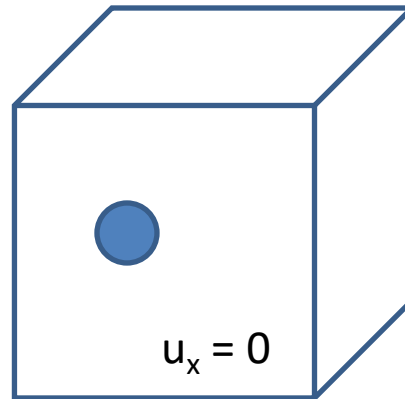
color represents u_x



Result is similar for $u_x = u_x/2$ ($We = We/4$)

Results of direct numerical simulation in Basilisk

free-slip BC

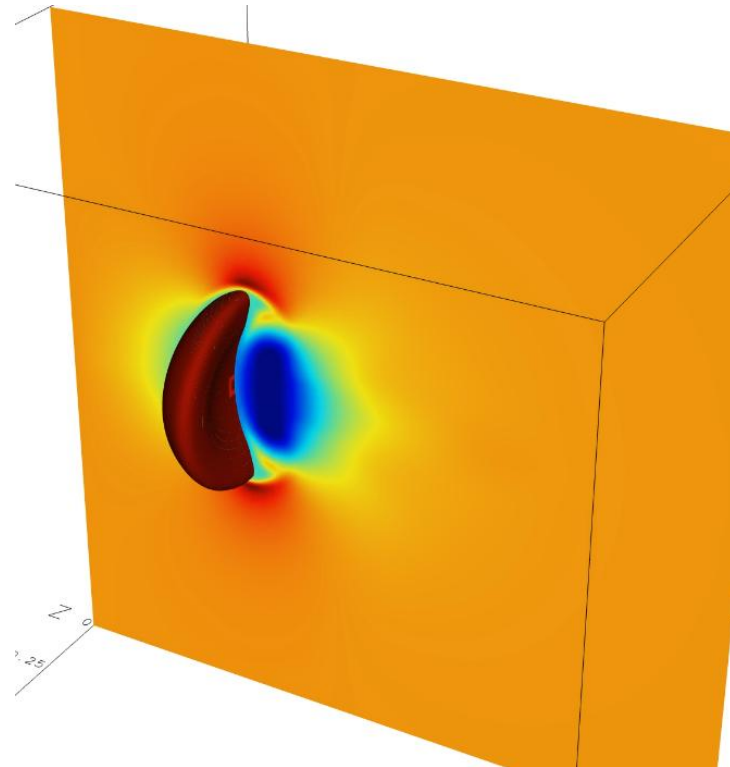
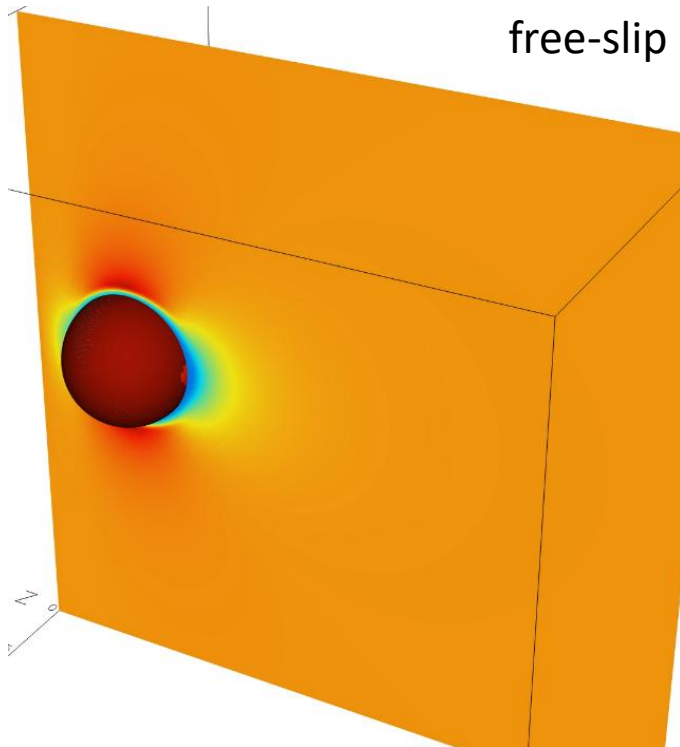


inflow BC
for u_x

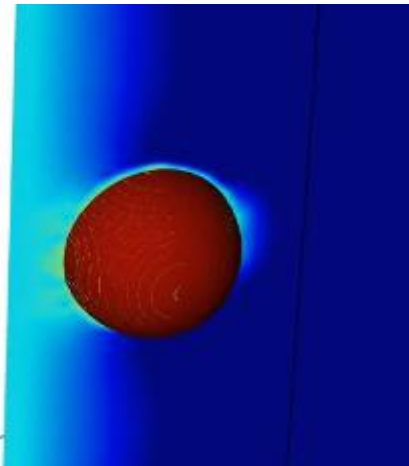
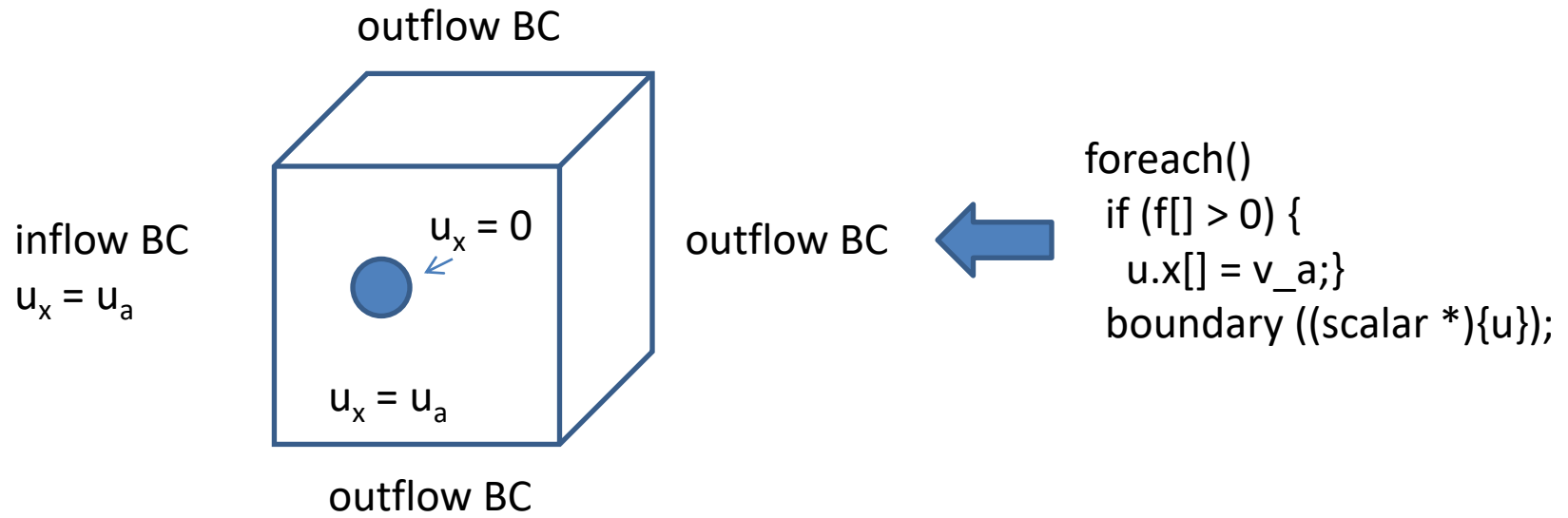
outflow BC

Level:
Initial – 6
Adaptive - 8

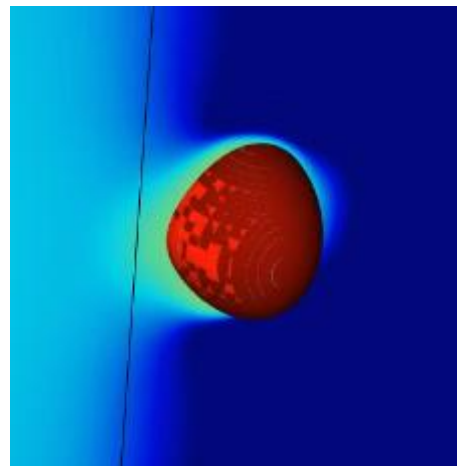
free-slip BC



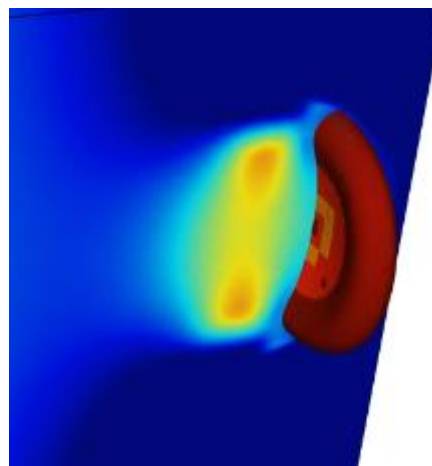
Results of direct numerical simulation in Basilisk



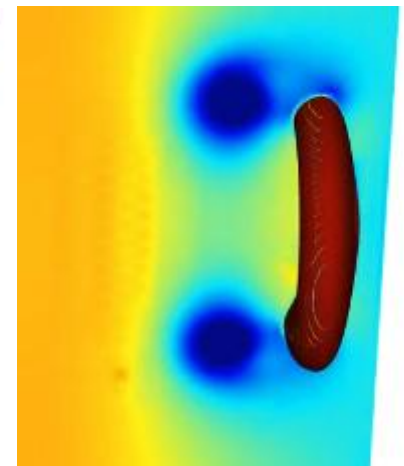
u_x



u_x



u_x



p

Issues

- The results are not the same in Gerris and in Basilisk – no bag-breakup in Basilisk
- Test simulation slows down, when core number > 18

Octree, 100 steps, **757.982 CPU**, 760.6 real, 5.29e+04 points.step/s, 34 var
8 procs, MPI: min 2e+02 (27%) avg 2.2e+02 (29%) max 2.3e+02 (30%)

Octree, 100 steps, **729.01 CPU**, 731.6 real, 5.5e+04 points.step/s, 34 var
10 procs, MPI: min 1.9e+02 (26%) avg 2.1e+02 (29%) max 2.5e+02 (34%)

Octree, 100 steps, **673.271 CPU**, 676.5 real, 5.95e+04 points.step/s, 34 var
18 procs, MPI: min 1.3e+02 (19%) avg 1.8e+02 (26%) max 2.1e+02 (31%)

Octree, 100 steps, **791.857 CPU**, 796.3 real, 5.06e+04 points.step/s, 34 var
24 procs, MPI: min 1.2e+02 (15%) avg 1.6e+02 (21%) max 1.9e+02 (24%)

Octree, 100 steps, **1356.3 CPU**, 1362 real, 2.96e+04 points.step/s, 34 var
36 procs, MPI: min 1.2e+02 (8.8%) avg 1.7e+02 (12%) max 2e+02 (15%)

Programs

Gerris

```
3 2 GfsSimulation GfsBox GfsGEdge {} {
  Time { end = 10. }
# Time { end = 0.1 }
# ApproxProjectionParams { tolerance = 1e-6 }
# ProjectionParams { tolerance = 1e-6 }

  EventBalance { istep = 1 } 0.1

  Refine 5

Global {
  #define RHO_L      1000.
  #define RHO_G      100.
  #define MU_L       1.003e-3
  #define MU_G       1.8e-5
  #define VAR(T,min,max) (min + CLAMP(T,0,1)*(max - min))
  #define RHO(T)      VAR(T, RHO_G/RHO_L, 1.)
  #define MUR(T)      VAR(T, MU_G/MU_L, 1.)
}

VariableTracerVOF T
VariableFiltered T1 T 1

VariableCurvature K T Kmax
SourceTension T 4.672*1e-4 K

InitFraction T (x*x + y*y + z*z - 0.2*0.2) {tx = -0.2}

AdaptVorticity { istep = 1 } { maxlevel = 9 cmax = 1e-2 }
AdaptFunction { istart = 5 istep = 10 } {
  cmax = 0.2
  maxlevel = 8
  cfactor = 2
} (T > 0 && T < 1 ? dL*Kmax : 0)
```

```
PhysicalParams { alpha = 1./RHO(T1) }
  SourceViscosity 100*16*1e-6*MUR(T1)
}

GfsBox {
  left = Boundary {
    BcDirichlet U 0.8
    BcDirichlet V 0.
    BcDirichlet W 0.
  }
  top = BoundaryOutflow
  bottom = BoundaryOutflow
  back = BoundaryOutflow
  front = BoundaryOutflow
}

GfsBox {
  top = BoundaryOutflow
  bottom = BoundaryOutflow
  back = BoundaryOutflow
  front = BoundaryOutflow
}

GfsBox {
  top = BoundaryOutflow
  bottom = BoundaryOutflow
  back = BoundaryOutflow
  front = BoundaryOutflow
  right = BoundaryOutflow
}

1 2 right
2 3 right
```

Basilisk

```
#include "grid/octree.h"
#include "navier-stokes/centered.h"
#include "vof.h"
#include "tension.h"
#include "view.h"
#include "two-phase.h"
#include "tag.h"

#define RHOR    10.          /** rho_a*100 */
#define MUR     55.6
#define sig     (4.672*1e-4) /** dimensionless */
#define vis_w   (16.*1e-6)  /** dimensionless */
#define rad     0.2
#define v_a     0.8        /** u/10 */
#define cx     (-0.2)
#define cy      0.
#define cz      0.
#define vis_w_new (vis_w*100.) /** mu_a*100, mu_w*100 */

u.n[left] = dirichlet(v_a);
u.t[left] = dirichlet(0.);
u.r[left] = dirichlet(0.);
p[left]   = neumann(0.);
pf[left]  = neumann(0.);
u.n[right] = neumann(0.);
p[right]  = dirichlet(0.);
pf[right] = dirichlet(0.);

/** At the walls there are outflow */
u.n[top]   = neumann(0.);
p[top]     = dirichlet(0.);
pf[top]    = dirichlet(0.);
u.n[bottom] = neumann(0.);
p[bottom]  = dirichlet(0.);
pf[bottom] = dirichlet(0.);
u.n[front] = neumann(0.);
p[front]   = dirichlet(0.);
pf[front]  = dirichlet(0.);
u.n[back]  = neumann(0.);
p[back]    = dirichlet(0.);
pf[back]   = dirichlet(0.);
```

```
/** The walls are free-slip */
/**u.n[top]   = neumann(0.);
u.t[top]     = neumann(0.);
u.n[bottom]  = neumann(0.);
u.t[bottom]  = neumann(0.);
u.n[front]   = neumann(0.);
u.t[front]   = neumann(0.);
u.n[back]    = neumann(0.);
u.t[back]    = neumann(0.);*/
```

```
int adaptmax;
```

```
int main() {
    L0 = 3.;
    origin (-0.5, -L0/2., -L0/2.);
    f.sigma = sig;
    TOLERANCE = 1e-6;
    rho1 = 1.;
    rho2 = 1./RHOR;
    mu1 = vis_w_new;
    mu2 = vis_w_new/MUR;
    init_grid (64);
    adaptmax = 8;
    run(); }
```

```
event init (t = 0) {
    if (!restore (file = "restart")) {
        /**if (!restore (file = "snapshot-1")) {*/
        refine (level < adaptmax &&
                sq(0.9*rad) - sq(x-cx) - sq(y-cy) - sq(z-cz) < 0.0 &&
                sq(1.1*rad) - sq(x-cx) - sq(y-cy) - sq(z-cz) > 0.0);
        fraction (f, - (sq(x-cx) + sq(y-cy) + sq(z-cz) - sq(rad)));
```

```
/** initial velocity */
```

```
foreach()
    if (f[] > 0) {
        u.x[] = v_a; }
    boundary ((scalar *){u});
    }
```

```
event adapt (i++) {
    double uemax = 1e-2;
    adapt_wavelet ({f,u}, (double[]){0.01,uemax,uemax,uemax}, adaptmax, 6); }
}
```